Miner Petrol (2012) 104:211–224
DOI 10.1007/s00710-011-0187-1

ORIGINAL PAPER

# The origin of mafic microgranular enclaves and their host granodiorites from East Kunlun, Northern Qinghai-Tibet Plateau: implications for magma mixing during subduction of Paleo-Tethyan lithosphere

**Fu-Hao Xiong · Chang-Qian Ma · Jin-Yang Zhang · Bin Liu**

Received: 14 February 2011 / Accepted: 10 November 2011 / Published online: 3 December 2011


**Abstract** Voluminous granodioritic magmatism is recorded in the East Kunlun, Northern Qinghai-Tibet Plateau. Here we present mineralogical, petrological, geochemical and Sr-Nd-Hf isotopic data and zircon U-Pb ages for the Naomuhun pluton and its numerous mafic microgranular enclaves (MMEs). Whole-rock geochemical data and regional geological studies indicate that this pluton consists of subduction-related high-K calc-alkaline metaluminous, I-type granodiorite. The MMEs have plagioclase xenocrysts and disequilibrium textures, such as oscillatory zoning and resorbed rims, indicating magma mixing. Compositions of plagioclase ($An_{30}$-$An_{49}$), amphibole (Mg#=0.62~0.68), and biotite (Mg#=0.52–0.56) of MMEs are similar to or very slightly different from equivalent minerals in the host granodiorites, suggesting nearly complete equilibration between the mafic-and felsic magmas. The zircon U-Pb age of the MMEs (263±2 Ma) is identical, within analytical error, to that of the host granodiorites (261±2 Ma). The MMEs have $\varepsilon_{Hf}(t)$ values of −6.83 to −3.15 (average=−4.68), whereas those of the granodiorites range from −9.00 to −3.20 (average −5.63), which is identical within analytical uncertainty. Combined with relatively homogeneous Sr-Nd isotopic compositions, we suggest the MMEs were derived from magma mixing, and their source is similar to an enriched mantle composition. The granodiorites have $T_{DM2}$(Hf) model ages ranging from 1.49 to 1.86 Ga, consistent with the Nd model ages ($T_{DM2}$), implying that the host magma was derived from Paleo- or Meso-proterozoic rocks, probably the Xiaomiao Group, which forms the basement of East Kunlun. We propose a model for magma formation and magma mixing in a subduction zone environment, in which subduction of an oceanic slab at ca. 260 Ma led to fluid metasomatism, inducing partial melting of an enriched lithospheric mantle to form the voluminous mafic magma. The mafic magma underplated the overlying lower crust, resulting in its partial melting to form felsic magma. The mafic magma then mixed with the felsic magma at lower crustal levels to form the MMEs by convective motion, or forceful injection into the host felsic magma. The MMEs and their host magma were then emplaced at a depth of ca. 12 km, where they crystallized at a temperature of ca. 700–770°C.

Editorial handling: J. G. Raith

**Electronic supplementary material** The online version of this article (doi:10.1007/s00710-011-0187-1) contains supplementary material, which is available to authorized users.

F.-H. Xiong · C.-Q. Ma
State Key Laboratory of Geological Processes and Mineral Resources, China University of Geosciences, 430074, Wuhan, People's Republic of China

F.-H. Xiong · C.-Q. Ma (✉) · B. Liu
Faculty of Earth Sciences, China University of Geosciences, 430074, Wuhan, People's Republic of China
e-mail: cqma@cug.edu.cn

J.-Y. Zhang
Faculty of Earth Resources, China University of Geosciences, 430074, Wuhan, People's Republic of China

## Introduction

Suprasubduction zones, commonly referred to as "subduction factories", play an important role in plate tectonics, melt generation and crustal evolution. The "subduction factory" is a metaphor for the geochemical interaction between four possible components, i.e., the subducted slab, mantle wedge, asthenospheric mantle and overlying crust (Defant and Drummond 1990; Hussain et al. 2004; McCulloch and Gamble 1991; Omrani et al. 2008; Stern and Kilian 1996;

Tatsumi and Kogiso 2003). This multi-source complex environment commonly leads to widespread magma mixing in subduction zones, such as that at Mount Shasta in northern California (Streck et al. 2007). However, most workers have focused on specific subduction-related rocks, such as adakite, high-magnesium andesite and arc lavas, when studying magma mixing in subduction zones (Anderson 1976; Debaille et al. 2006; Pal et al. 2007; Streck et al. 2007), ignoring the significance of mafic microgranular enclaves (MMEs) in subduction zone magmatism. MMEs are common in calc-alkaline granitoids and can provide important information on the nature of the magma source and the generation of the granitic melt. They are valuable means for studying mixing of crustal and mantle magmas (Arvin et al. 2004; Castro et al. 2006; Ma et al. 1992; Qin et al. 2010; Yang et al. 2007a), but little work in this respect has been done on subduction-related granitoids and their enclaves (e.g. Parada et al. 1999), and their geochemical characteristics and genesis are still poorly understood.

In the Northern Qinghai-Tibet Plateau, owing to the northeastward subduction of Paleo-Tethyan oceanic lithosphere beneath East Kunlun, voluminous Late Permian-Middle Triassic (260–245 Ma) arc magmatism occurred (Harris et al. 1988; Mock et al. 1999; Yang et al. 1996), which is recorded by calc-alkaline granitoids. These granitoids contain abundant MMEs, making East Kunlun a natural laboratory for the study of magma mixing in subduction zone environments. Although numerous studies have been carried out on the MMEs in East Kunlun, all focused exclusively on those found in syn-collisional (245–220 Ma) rocks (Liu et al. 2002; Liu et al. 2004; Chen et al. 2005). Thus, little is known about the origin of the East Kunlun subduction-related magmatic rocks and their MMEs, and the role that these rocks played in the evolution of Paleo-Tethys in the Qinghai-Tibet Plateau. Here, we report the results of a detailed study of the subduction-related MMEs in the East Kunlun orogenic belt, using zircon U-Pb geochronology, petrography, mineralogy, whole-rock geochemistry and Sr-Nd-Hf isotope geochemistry.

## Geological setting

The East Kunlun orogenic belt, located in the Northern Qinghai-Tibet Plateau, is bounded by the Qaidam basin to the north, the Bayan Har-Songpan Ganzi block to the south, the Qinling-Dabie orogenic belt to the east and the NE-trending Altyn Tagh Fault to the west (Fig. 1a). The East Kunlun orogenic belt is part of the Paleo-Tethyan tectonic domain. The A'nyemaqen part of Paleo-Tethys began to subduct beneath the Kunlun terrane in the Late Permian, and the ocean finally closed in the early-middle Triassic, forming the A'nyemaqen Paleo-Tethys suture zone (Fig. 1a). Due to subduction of the Paleo-Tethyan lithosphere and subsequent collision, the East Kunlun orogenic belt was a region of large-scale, late Permian to late Triassic magmatism (Chen and Wang 1996; Konstantinovskaia et al. 2003; Yang et al. 1996; Yang et al. 2009).

In this study, we focus on the Naomuhun (NMH) pluton, located in the eastern section of East Kunlun (Fig. 1a), about 10 km south of Balong Township. The NMH pluton intruded four basement complexes: (1) the Paleoproterozoic Baishahe Group, consisting of banded amphibolite, mica plagioclase gneiss, granulite, banded marble, mica schist and mica quartz schist; (2) the Middle Proterozoic Xiaomiao Group, composed mainly of quartzite, mica quartz schist, biotite plagioclase gneiss and marble; (3) the Neoproterozoic Wanbaogou Group, which contains various combinations of clastic rocks, volcanic rocks and carbonates; and (4) the Lower Paleozoic Nachitai Group, which consists of volcanic lava, tuff, tuffaceous phyllite, slate, sandstone, schist, and carbonates. The pluton crops out discontinuously for about 50 km in an E-W direction over an area of ~364 $km^2$ (Fig. 1b). It consists mainly of biotite granodiorite with abundant MMEs.

## Sampling and petrography

One sample each of the granodiorite (BL13) and the mafic enclaves (BL13-1) were collected for zircon dating at N35° 49.665′, E97°24.639′ (Fig. 1b).

The medium-grained granodiorite consists of plagioclase (40–45 vol.%), quartz (20–25 vol.%), potassium feldspar (10–15 vol.%), biotite (5 vol.%) and amphibole (5 vol.%). The accessory minerals are titanite, apatite, zircon, epidote and opaque minerals.

The MMEs form dense swarms and range from submillimeter up to a meter in size and are they angular to ovoid in shape (Fig. 2a). Most of the MMEs are texturally and mineralogically similar to their host rocks, consisting of plagioclase (45–50 vol.%), biotite (15–20 vol.%), euhedral amphibole (5–10 vol.%), anhedral quartz (10–15 vol.%) and <5% accessory minerals, including acicular apatite, zircon, and sphene. Many of the MMEs contain small, subhedral feldspar xenocrysts (Fig. 2b).

The MMEs contain disequilibrium textures, such as plagioclase with oscillatory zoning (Fig. 2c), poikilitic plagioclase rimmed by mafic minerals (Fig. 2d), and euhedral hornblende with inclusions of plagioclase and biotite (Fig. 2e and f).

## Analytical methods

The samples for dating were collected from fresh outcrops, and the zircons were separated by heavy liquids and using a

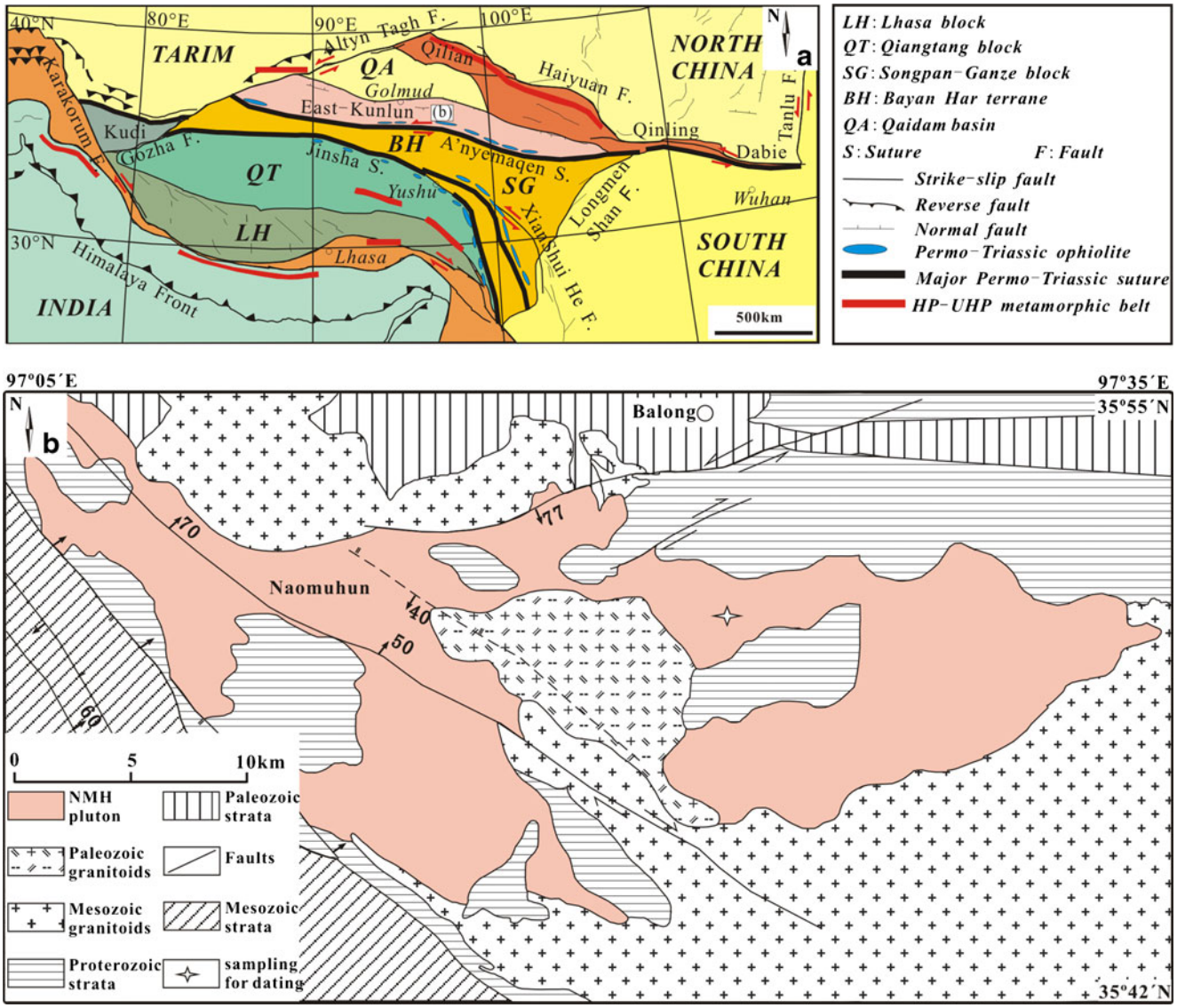


**Fig. 1** **a** Tectonic outline of the Tibetan Plateau showing the study area (after Roger et al. 2008); **b** Simplified geological map of Naomuhun pluton (after Wang et al. 2003)

Frantz magnetic separator. Before analysis, the zircon grains were photographed with an optical microscope, and the internal structures of the polished grains were observed in cathodoluminescence (CL).

The U-Pb dating of zircon was done by LA-ICP-MS at the State Key Laboratory of Geological Processes and Mineral Resources (GPMR), China University of Geosciences, Wuhan. Laser sampling was performed using a GeoLas 2005 System with a spot size of 32 μm. An Agilent 7500a ICP-MS instrument was used to acquire ion-signal intensities. Nitrogen was added into the central gas flow (Ar+He) of the Ar plasma to increase sensitivity and improve precision (Hu et al. 2008). Off-line selection and integration of background and analyte signals, and time-drift correction and quantitative calibration for U-Pb dating were performed by the software *ICPMSDataCal* (Liu et al. 2008). Concordia diagrams and weighted mean calculations were made using Isoplot/Ex_ver3 (Ludwig 2003). Besides, the data less than 95% concordance were completely rejected. Detailed operating conditions for the laser ablation system and the ICP-MS instrument were the same as described by Zong et al. (2010).

In order to check the data quality, two reference materials, i.e., zircons 91500 and GJ-1, were analysed and yielded weighted mean $^{206}Pb/^{238}U$ ages of 1062±3 Ma ($n$=24, 2σ) and 599±4 Ma ($n$=8, 2σ), respectively, which are in good agreement with the recommended ages of 1065 Ma (Wiedenbeck et al. 1995) and 600 Ma (Jackson et al. 2004). Reported uncertainties were propagated by quadratic addition of the external reproducibility obtained from the standard zircon GJ-1 during individual analytical sessions and the within-run precision of each analysis.

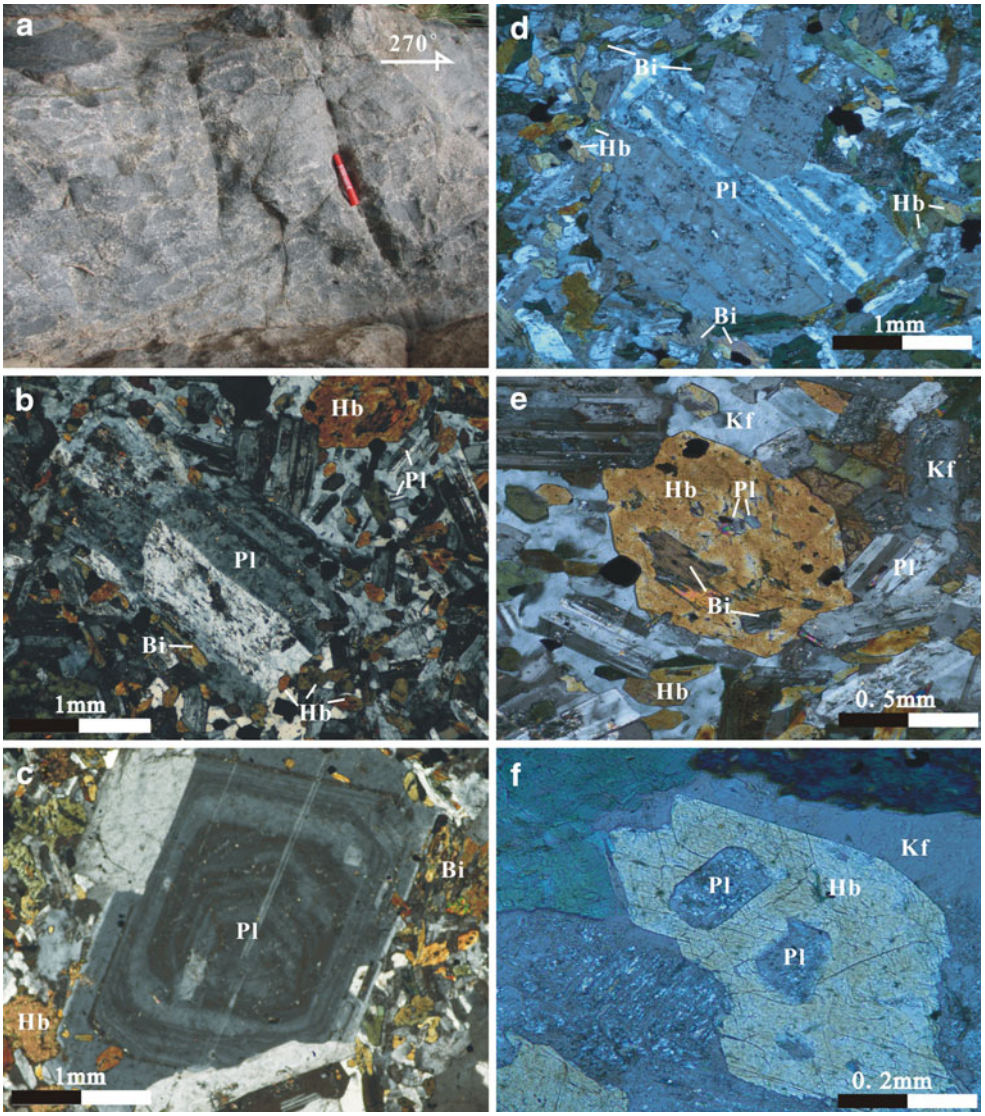


**Fig. 2** Field and thin section photographs of various disequilibrium textures in the NMH mafic microgranular enclaves (MMEs). **a** Enclave swarms in the NMH pluton; **b** Plagioclase xenocryst in the MME; (**c**) Oscillatory zoned plagioclase; **d** Plagioclase xenocryst rimmed by biotite and hornblende; **e** subhedral hornblende with inclusions of plagioclase and biotite; **f** subhedral hornblende with inclusions of plagioclase

Zircon Hf isotopic analysis was performed on the dated zircon grains using an excimer (193 nm wavelength) laser ablation inductively coupled plasma mass spectrometer (LA-MC-ICP-MS) system at the State Key Laboratory of Continental Dynamics, Northwest University, Xi'an, China. A beam diameter of 44 μm was used in this study with a laser pulse frequency of 10 Hz, and the analysis was placed close to the U-Pb dating spot, either overlapping the dating spot or into the same zone (Figs. 3a and 4a). The $^{176}Lu/^{175}Lu$ ratio of 0.02669 and $^{176}Lu/^{172}Yb$ ratio of 0.5886 were used to calculate $^{176}Lu/^{177}Hf$ and $^{176}Hf/^{177}Hf$ (Bievre and Taylor 1993; Chu et al. 2002). Zircon 91500, GJ-1 and MON-1 were used as the reference for calibration and controlling the condition of analytical instrumentation, which yielded weighted mean $^{176}Hf/^{177}Hf$ ratios of 0.282299±0.000021 ($n$=9, 2σ), 0.282012±0.000029 ($n$=9, 2σ) and 0.282742±0.000007 ($n$=9, 2σ), respectively. These results are in good agreement with the recommended $^{176}Hf/^{177}Hf$ ratios of 0.282296, 0.282015 and 0.282739 for the three reference materials (Elhlou et al. 2006; Woodhead and Hergt 2005). The detailed analytical technique for this method was described by Yuan et al. (2008).

Mineral compositions were analyzed using a JEOL-JXA-8100 electron microprobe at GPMR, China University of Geosciences, Wuhan, using the analytical procedures described by Zheng et al. (2009). Whole-rock major element analyses were carried out using a Rigaku 3080E1-type XRF spectrometer at the Bureau of Geology and Mineral Resources, Hubei Province, China, with analytical precision better than 5%. Trace element, including REE and Sr-Nd isotope analyses were conducted by LA-ICP-MS and Finnigan Triton thermo-ion mass isotope spectrometer at the GPMR Laboratory, respectively. USGS standards AGV-2, BHVO-2 and BCR-2 were used for trace elements calibration (Liu et al. 2008). The preferred values of trace element concentrations for the USGS reference glasses are from the GeoReM database (http://georem.mpch-mainz.gwdg.de/). The analytical accuracies were better than 5%

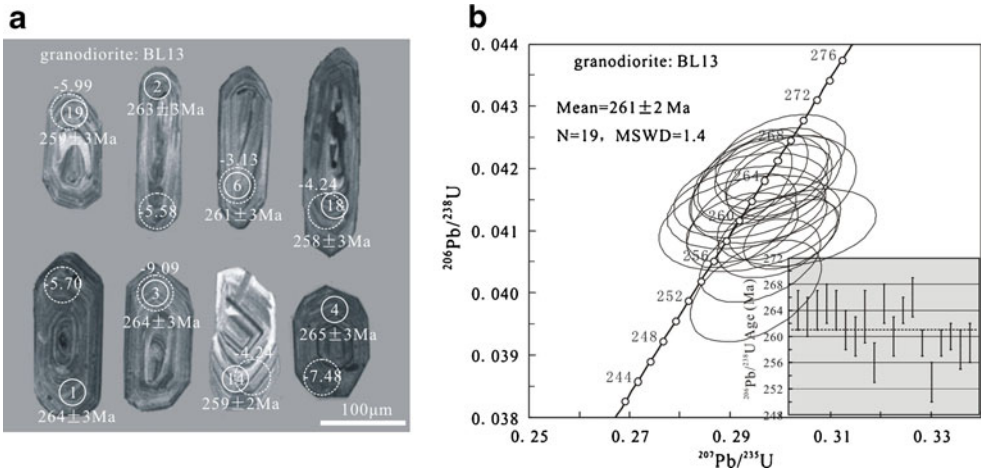


**Fig. 3** **a** Representative CL images of zircons (*solid circles* and *dashed circles* represent the points for U-Pb and Lu-Hf isotope analysis, respectively) and **b** zircon U-Pb concordia diagram from NMH granodiorite (sample BL13)

for Co, Ni, Ga, Rb, Y, Zr, Nb, Hf, Ta and light REE, and 5–12% for the remaining elements. The mass fractionation corrections for Sr and Nd isotopic ratios were based on $^{86}Sr/^{88}Sr=0.1194$ and $^{146}Nd/^{144}Nd=0.7219$, respectively. The average $^{143}Nd/^{144}Nd$ ratio of the La Jolla standard measured during the sample runs is 0.511862±5 (2σ), whereas the NBS-987 standard gave $^{87}Sr/^{86}Sr$ as 0.710236±16 (2σ). The analytical instruments and detailed operating conditions for the trace element and Sr-Nd isotope analyses are the same as those described by Gao et al. (2004).

## Results

### Zircon U-Pb ages

The zircons selected for analysis from the granodiorite and its MMEs are transparent colorless to pale yellow, euhedral columnar crystals without inclusions. The grains are 80 to 120 μm long, with width/length ratios of about 1:2–5. All of the zircons show typical oscillatory zoning in the CL images (Fig. 3a and 4a), indicating that they are of magmatic origin (e.g. Corfu et al. 2003; Hoskin and Schaltegger 2003; Wu and Zheng 2004).

The results of U-Pb dating of zircon from the granodiorite (sample BL13) and MMEs (sample BL13-1) are listed in Supplementary Table 1. The zircons have high concentrations of Th and U (average, 456 and 511 ppm, respectively) and Th/U ratios (0.5–1.5). A total of 19 concordant U-Pb analyses were obtained from BL13, with $^{206}Pb/^{238}U$ ages ranging from 253±3 to 266±3 Ma and yielding a weighted mean $^{206}Pb/^{238}U$ age of 261±2 Ma with an MSWD of 1.4 (confidence intervals are always reported at 95% confidence level; Fig. 3b). We interpret the weighted mean age as the emplacement age of the NMH granodiorites, which formed close to the Middle-Upper Permian boundary.

Zircon ages of the MME (BL13-1) are concordant within analytical uncertainties, with $^{206}Pb/^{238}U$ ages ranging from 256±3 to 268±3 Ma (1σ, Supplementary Table 1). Nineteen analyses provided a weighted average age of 263±2 Ma (MSWD=1.9, 95% confidence limit; Fig. 4b), which is within analytical uncertainty identical to the age of the granodiorite. This suggests that the granodiorites and

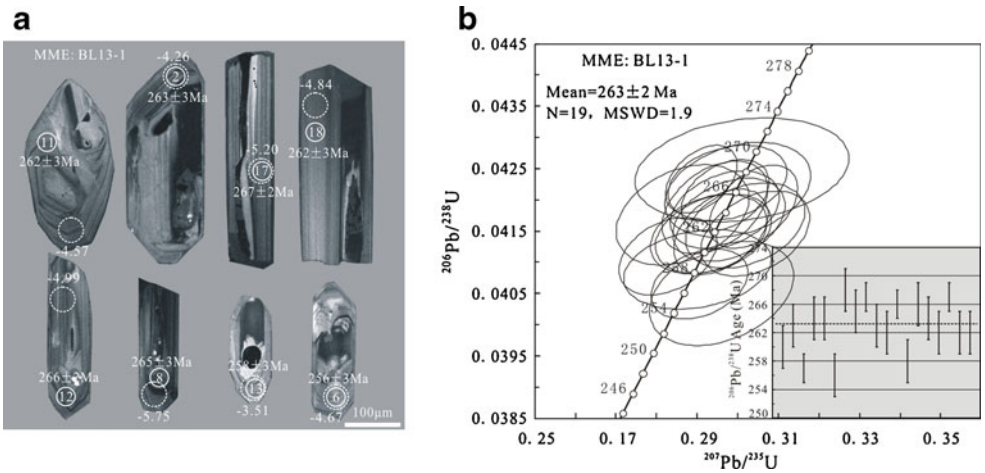


**Fig. 4** **a** Representative CL images of zircons (the *solid circles* and *dashed circles* represent the points for U-Pb and Lu-Hf isotope analysis, respectively) and **b** zircon U-Pb concordia diagram from NMH MMEs (sample BL13-1)

MMEs formed at the same time, and that they are petrogenetically linked.

## Mineral chemistry

A careful selection of plagioclase, K-feldspar, biotite and amphibole was done under optical microscope prior the electron microprobe analysis, in which the $Fe^{2+}$ and $Fe^{3+}$ values of hornblende and biotite were calibrated after Lin and Peng (1994).

### *Feldspar*

Compositions of plagioclase and K-feldspar from the granodiorites and MMEs are given in Supplementary Table 2. Plagioclase is of andesine composition with $An_{30}$-$An_{49}$ in the MMEs and $An_{30}$-$An_{44}$ in the host granodiorites (Fig. 5; Supplementary Table 2). Likewise, the K-feldspar in both the MMEs and granodiorites is orthoclase, with Or component between 91–95% (Supplementary Table 2). Zoned-plagioclase in the MMEs is slightly more anorthitic in the core than in the rim, whereas in the granodiorites the rims are typically richer in anorthite than the cores (Supplementary Table 2). This reverse zoning of plagioclase in the granodiorite could be interpreted as evidence of mixing between silicic and mafic magmas (Ginibre et al. 2007; Pietranik and Koepke 2009; Slaby and Götze 2004).

### *Amphibole*

Representative analyses of amphiboles from both rock types are given in Supplementary Table 3. Most of the amphiboles can be classified as calcic magnesiohornblende (Leake et al. 1997), with a few actinolitic hornblendes in the MMEs (Fig. 6). The amphiboles in the MMEs and host

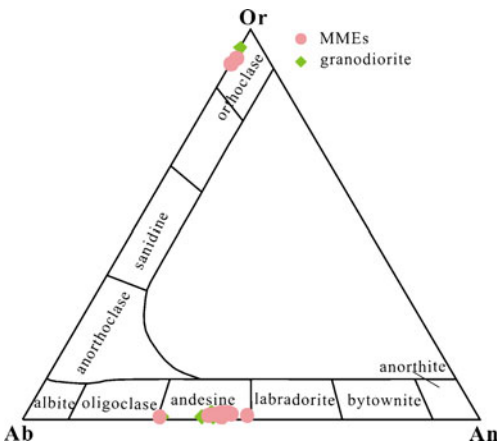


**Fig. 5** Chemical compositions of feldspars from the host rocks and MMEs in NMH pluton

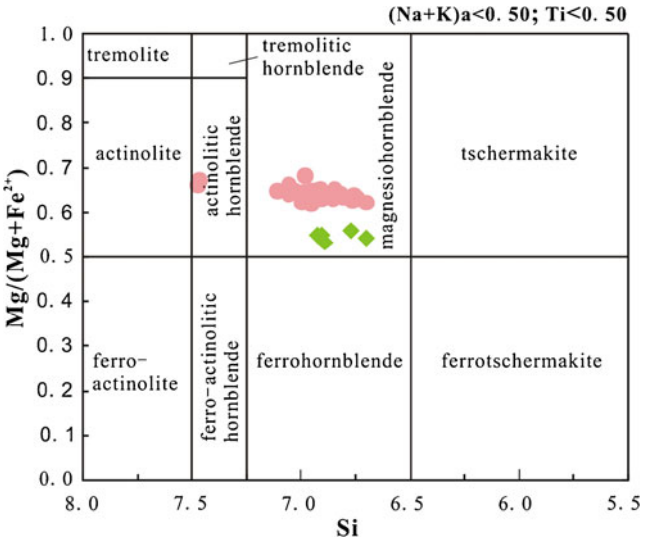


**Fig. 6** Composition and classification (Leake et al. 1997) of amphiboles from the host rock and MMEs in East Kunlun. Same symbols as in Fig. 5

rocks are very similar, but those in the MMEs have slightly higher Mg# [(Mg#=atomic ratios Mg/(Mg+Fe), where Fe is total iron)] (0.62–0.68) than those in the granodiorites (0.53–0.56). Few calcic amphibole crystals are zoned with a magnesiohornblende core and an actinolite rim (Supplementary Table 3; Fig. 6), which are interpreted as marking progressive oxidation in the magmatic environment (Martin 2007). The amphiboles have medium $SiO_2$ contents, and low $TiO_2$ and $Na_2O+K_2O$, similar to those from calc-alkaline igneous rocks in subduction environments (Coltorti et al. 2007; Martin 2007).

### *Biotite*

All biotite crystals are uniform in composition, magnesian in character and plot within the calc-alkaline field in the MgO-$FeO^T$-$Al_2O_3$ diagram (Supplementary Table 4; Fig. 7a and b). The $FeO^T$/MgO ratios of the biotites in the MMEs (1.66–1.91) are identical to those in the host granodiorites (1.78–2.03), suggesting complete equilibration between the respective biotites. Furthermore, the studied biotite is similar in composition to that commonly found in calc-alkaline (mostly subduction-related), I-type granitoids (Abdel-Rahman 1994).

### *P-T conditions of crystallization*

Various aluminum-in-hornblende geobarometers (Supplementary Table 5) were used to estimate the pressures under which the MMEs and their host granitoids formed, because all the rocks contain the required phase assemblage (quartz+plagioclase+K-feldspar+hornblende+biotite+apatite+zircon+titanite). In addition, we use the hornblende-plagioclase thermometer to calculate the crystallization temperatures of

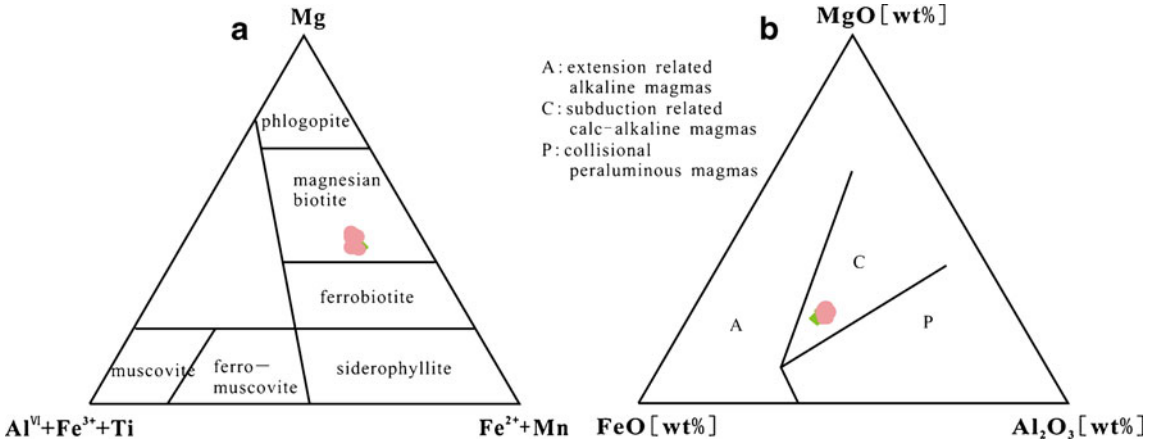


**Fig. 7** **a** Mg-($Al^{VI}$+$Fe^{3+}$+Ti)-($Fe^{2+}$+Mn) diagram (Forster 1960) and **b** MgO-FeO-$Al_2O_3$ diagram (Abdel-Rahman 1994) for biotite from host rocks and MMEs in East Kunlun. Same symbols as in Fig. 5

the studied rocks. Based on these calculations, the MMEs and their host granodiorites crystallized under the same P-T conditions (Supplementary Table 5). The pressures (3.2–3.4 kbar) calculated from the geobarometer of Schmidt (1992) correspond to shallow depths of ~12 km. Using the thermometers of Blundy and Holland (1990), the calculated equilibrium temperature of the co-existing hornblende and plagioclase in the MMEs (706–771°C, average=737°C) is essentially identical to that in the host rocks (729–761°C, average=742°C; Supplementary Table 5).

## Whole-rock geochemistry

Whole-rock geochemical data are presented in Supplementary Table 6. Most of the granodiorite samples plot consistently in the granodiorite field on the classification diagram of Middlemost (1994), whereas the MMEs plot in the monzodiorite field (not shown). The MMEs and granodiorites both are high-K, calc-alkaline and metaluminous to slightly peraluminous rocks with A/CNK ranging from 0.75 to 1.05 (Supplementary Table 6), similar to I-type granite (Fig. 8a and b).

Chondrite-normalized REE patterns of the MMEs and granitoid rocks are invariably enriched in light REE (LREE) with respect to the HREE [$(La/Yb)_N$=4.22–4.47 and 9.84–17.02 for MMEs and granodiorites], and all samples display moderately negative Eu anomalies (δEu=0.50–0.87; Supplementary Table 6; Fig. 9a). In the primitive mantle-normalized spidergram (Fig. 9b), all of the samples are enriched in large ion lithophile elements (LILE), such as Rb, Ba, Tu, U, K, and are depleted in high field strength elements (HFSE) Nb, Ta, P, Ti, typical of subduction-related magmatic rocks (Brown et al. 1984; Hussain et al. 2004; Omrani et al. 2008; Wade et al. 2006).

## Sr-Nd-Hf isotope geochemistry

Whole-rock Sr-Nd isotopic compositions for the MMEs and their host granodiorites are given in Supplementary Table 6 with initial ratios calculated at an age of 262 Ma. The MMEs and granodiorites have relatively homogeneous isotopic compositions, with high initial Sr ratios [$(^{87}Sr/^{86}Sr)_i$=0.70850–0.70863] and low εNd(t) values (εNd(t)=−6.1 to −4.6). The MMEs and granodiorites have

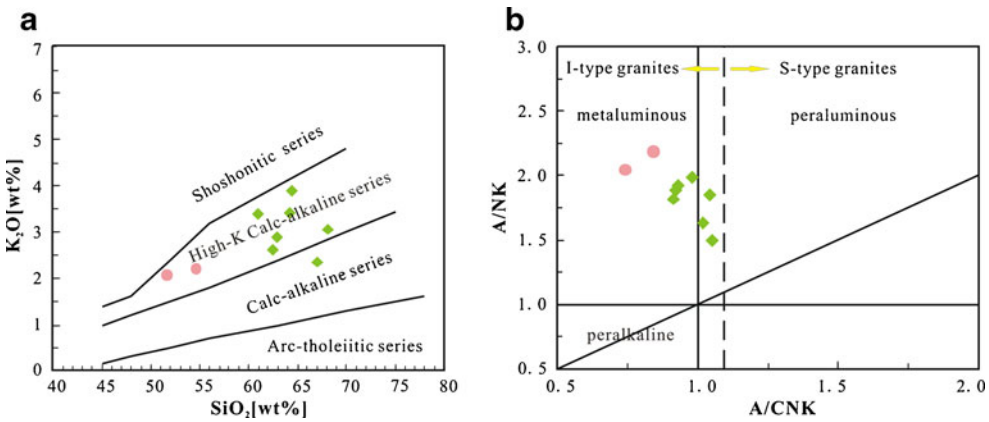


**Fig. 8** Chemical classifications of the NMH granodiorites and MMEs. **a** $K_2O$ vs $SiO_2$ diagram (Peccerillo and Taylor 1976); **b** A/NK vs A/CNK diagram (Chappel and White 1974; Maniar and Piccoli 1989). Same symbols as in Fig. 5

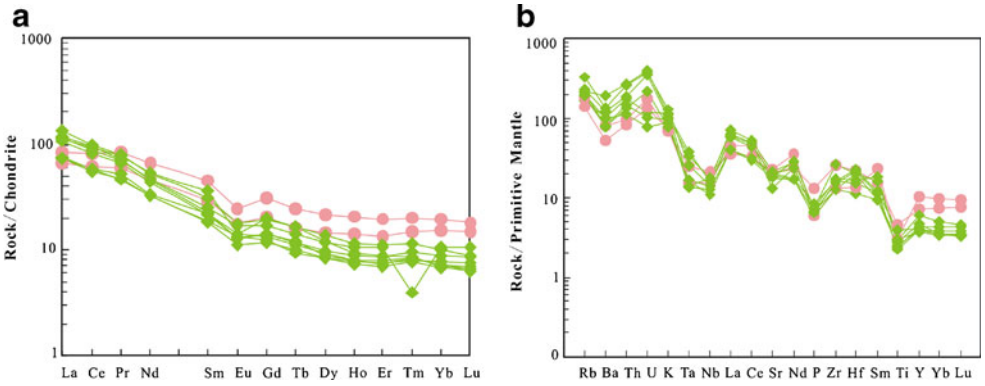


**Fig. 9** **a** Chondrite-normalized REE patterns and **b** Primitive mantle-normalized element spider diagrams for MMEs and granodiorites. Chondrite REE abundances are after Taylor and Mclennan (1985), Trace element abundances for the primitive mantle are after Sun and Mcdonough (1989). Same symbols as in Fig. 5

similar Nd model ages ($T_{DM2}$), ranging between 1.40 and 1.52 Ga.

Zircons from the MMEs have similar initial $^{176}Hf/^{177}Hf$ values to those of the host granodiorites (average $(^{176}Hf/^{177}Hf)_i$=0.282478 in the MMEs and 0.282451 in the granodiorites; Supplementary Table 7). However, the $\varepsilon_{Hf}(t)$ values of granodiorites have a wider spread (Fig. 10). The MMEs have $\varepsilon_{Hf}(t)$ values ranging from −6.83 to −3.15, with a weighted mean of −4.68, while the $\varepsilon_{Hf}(t)$ values of granodiorites range from −9.00 to −3.20, with a weighted mean of −5.63. Two-stage model ages ($T_{DM2}$) are calculated for the source rock of the magma (Supplementary Table 7) by assuming a mean $^{176}Lu/^{177}Hf$ value of 0.015 for an average continental crust (Griffin et al. 2002). The granodiorites and MMEs have $T_{DM2}$ model ages ranging from 1.49 to 1.86 Ga (Supplementary Table 7; Fig. 10b), which is in accordance with their Sr-Nd isotopic compositions.

## Discussion

### Petrogenesis of the mafic microgranular enclaves

The MMEs have igneous mineralogy and textures, with feldspar xenocrysts and disequilibrium features such as oscillatory zoning, resorbed rims, poikilitic plagioclase, and acicular apatite, all of which are interpreted as reflecting chemical and/or thermal changes in the melt during crystal growth (Baxter and Feely 2002; Grogan and Reavy 2002). The enclaves in the NMH pluton commonly occur as swarms, which is an indication of mafic magma injection into felsic magma during magma mixing (Arvin et al. 2004; Blundy and Sparks 1992; Tobisch et al. 1997). Magma mixing is further supported by mineral chemistry, particularly the similarity in anorthite content of plagioclase between the MMEs and host rocks. The cores of plagioclase xenocrysts in the MMEs are identical in composition to the plagioclase in the felsic host rocks ($An_{30}$), but the rims are more calcic ($An_{49}$) (Supplementary Table 2). Such a compositional change suggests that the plagioclase xenocrysts were mechanically transferred from felsic magma into the mafic magma where a new and more calcic plagioclase overgrew the cores. In addition, some

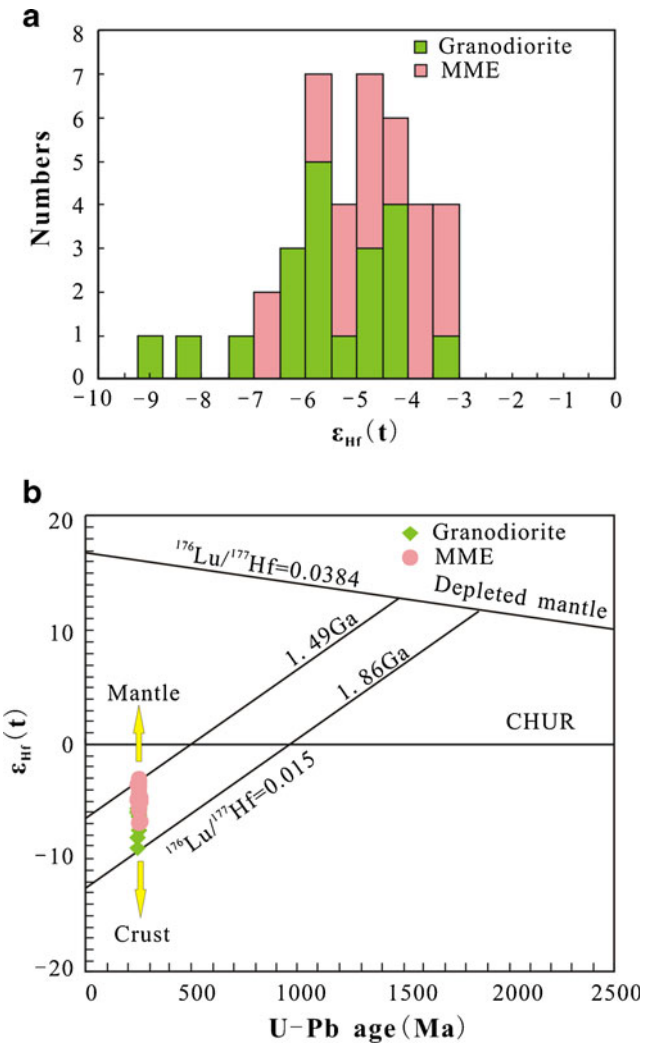


**Fig. 10** **a** Histogram of $\varepsilon_{Hf}(t)$ and **b** Plots of $\varepsilon_{Hf}(t)$ vs U-Pb ages for zircons from sample BL13-1 and BL13 (the values used for constructing the DM and crust reference evolution lines are after Griffin et al. (2000, 2002))

plagioclase grains from the felsic host rocks have sodium-rich cores ($An_{30}$), which are overgrown by calcium-rich zones ($An_{40}$)(Supplementary Table 2). This relationship is interpreted as the result of mixing between mafic and felsic magmas. Preservation of the compositional and textural disequilibrium features in the plagioclase is interpreted to be due to rapid crystallization and incomplete mixing.

The MMEs have P-T conditions of crystallization similar to those of their host rocks (MMEs: average 737°C and 3.15 kbar; host rocks: average 742°C and 3.39 kbar), showing that they crystallized together. In addition, the MMEs and host granodiorites have identical mineral assemblages, similar mineral compositions, similar geochemical characteristics, indistinguishable Sr-Nd isotopic compositions and an almost coeval crystallization age, also compatible with magma mixing. The wide range in zircon Hf isotopic compositions of the MMEs and granodiorites precludes a simple evolution by closed-system fractionation, because such mechanisms cannot produce the variable Hf isotopic compositions. On the other hand, such compositions can be explained by magma mixing because such a process can produce zircons with homogeneous U-Pb ages and variable Hf isotopic compositions (Yang et al. 2006; Yang et al. 2007b).

## Magma sources and tectonic implications

Whole-rock geochemical data show that the NMH pluton is composed of metaluminous, high-K, calc-alkaline, I-type granodiorite (Fig. 8). All of the rocks are enriched in LILE and depleted in HFSE, characteristics typical of subduction-related magmatic rocks (Brown et al. 1984). A subduction-related origin for these rocks is consistent with their position in tectonic discrimination diagrams (Fig. 11), and is consistent with the geological evolution of East Kunlun. The A'nyemaqen Paleo-Tethyan ocean opened at least as early as Late Carboniferous (308 Ma), and closed during the late Permian-early Triassic (260–245 Ma), resulting in voluminous subduction-related magmatism in East Kunlun

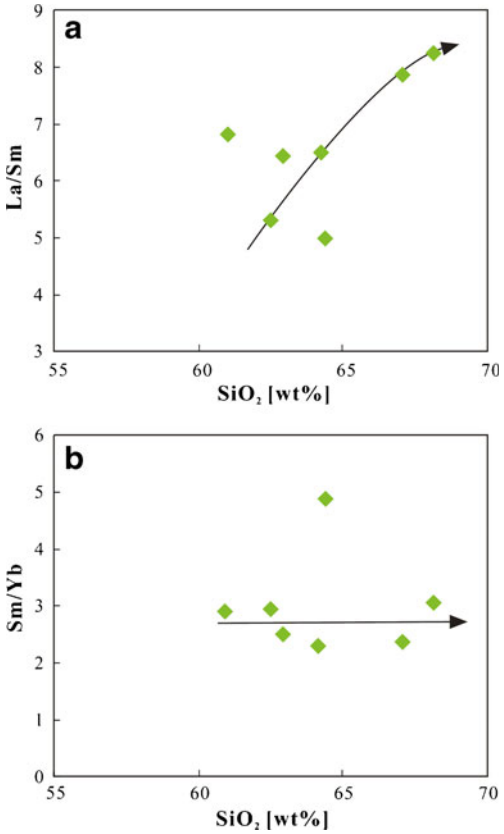


**Fig. 12** **a** La/Sm and **b** Sm/Yb vs. $SiO_2$ for the granodiorites in East Kunlun. Same symbols as in Fig. 5

(Bian et al. 2004; Harris et al. 1988; Jiang et al. 1992; Mock et al. 1999; Xu et al. 2007; Yang et al. 1996; Yang et al. 2005).

However, subduction-related, calc-alkaline magmatism may reflect a combination of processes, including melting of continental crust, the subducted slab and the mantle. We suggest that the NMH granodiorites formed by partial melting of continental crust. The granodiorites have relatively low ratios of $K_2O/Na_2O$, $(Na_2O+K_2O)/(FeO_{tot}+MgO+TiO_2)$, and $Al_2O_3/(FeO_{tot}+MgO+TiO_2)$ and high ratios of CaO/(MgO+FeO), characteristics, which are

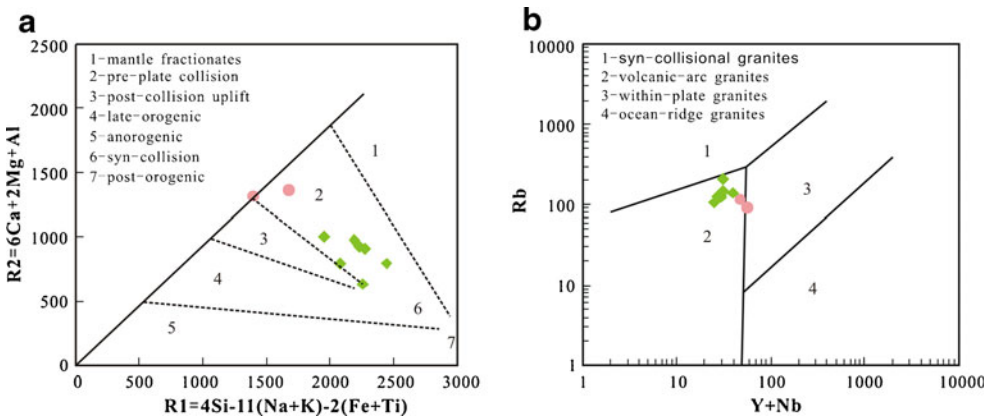


**Fig. 11** **a** Major element plot after Batchelor and Bowden (1985) and **b** Rb vs Y+Nb plot for the MMEs and granodiorites in East Kunlun (after Pearce et al. 1984). Same symbols as in Fig. 5

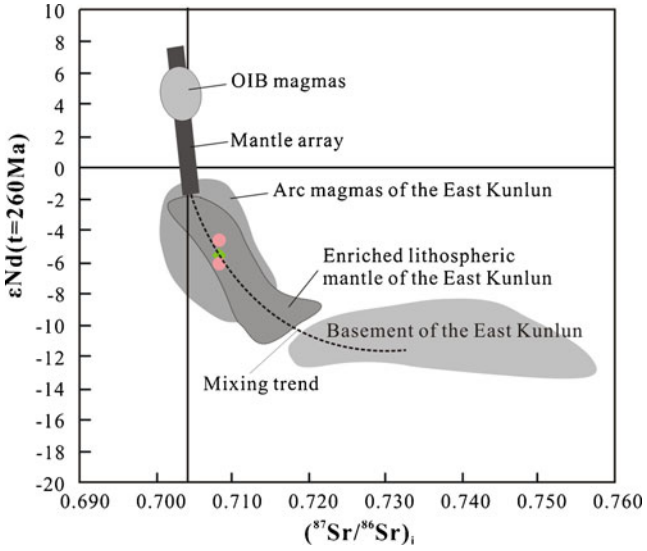


**Fig. 13** Correlation diagram between $(^{87}Sr/^{86}Sr)_i$ and εNd($t$=260 Ma) for NMH pluton (the data for the basement of East Kunlun is from Yu et al. 2005; data for enriched lithospheric mantle is from Chen et al. 2011; data for arc magmas is from Liu et al. 2003; Chen et al. 2007 and Yuan et al. 2009; data for OIB magmas is from Ma et al. 2007). Same symbols as in Fig. 5

consistent with the experimental data (not shown, Gardien et al. 1995; Patiño Douce 1997; Rapp and Watson 1995), suggesting that all of these rocks may be derived from dehydration melting of the lower crust. The depletion of Nb and Ta relative to LILE and LREE reflects retention of Ti-rich minerals (e.g. rutile) or hornblende in the residue because such minerals have high partition coefficients for Nb and Ta (Baier et al. 2008; Green and Pearson 1987; Green 1995; Kalfoun et al. 2002). The granodiorites show enrichment in LREE with respect to the HREE [$(La/Yb)_N$= 9.84–17.02], which suggests equilibrium with amphibole or garnet. Besides, the increasing trend between La/Sm ratio and $SiO_2$ content, together with the absence of a corresponding trend for Sm/Yb vs $SiO_2$ (Fig. 12), support the presence of amphibole as a residual phase in the crustal source of the felsic magmas. Partial melting of mafic lower crust is also consistent with the isotopic data. In fact, the whole-rock Nd model ages (1.40–1.52 Ga) and Hf model ages ($T_{DM2}$) of zircons from the NMH granodiorites ranging from 1.49 to 1.86 Ga, which are consistent with the ages of the East Kunlun basement rocks, i.e., the Proterozoic Xiaomiao Group (Wang et al. 2003; Xu et al. 2007), suggest their derivation from a major late Paleo-proterozoic crustal source (Fig. 10b).

The negative εHf(t) values (average: −5.63 and −4.68 for granodiorites and MMEs, respectively) suggest that old crustal materials or enriched lithospheric mantle played a significant role in the magma generation, consistent with the Sr-Nd isotope data. Importantly, the Sr-Nd-Hf isotopic composition of MMEs is identical to those of granodiorite, which suggest mixing between a crustal magma and a mantle-derived component.

We further suggest that the mafic end-member involved in the magma mixing was derived from enriched lithospheric mantle, rather than asthenospheric mantle, because all the rocks have much lower values of siderophile elements (Co: 5–23 ppm, Ni: 3–50 ppm, Cu: 3–80 ppm) than rocks derived from asthenospheric mantle, and have enriched Sr-Nd-Hf isotopic compositions, which are incompatible with derivation from the asthenospheric mantle. The Sr-Nd isotope data plotted in Fig.13 illustrate that the MMEs are typical of an enriched lithospheric mantle as the major component of the

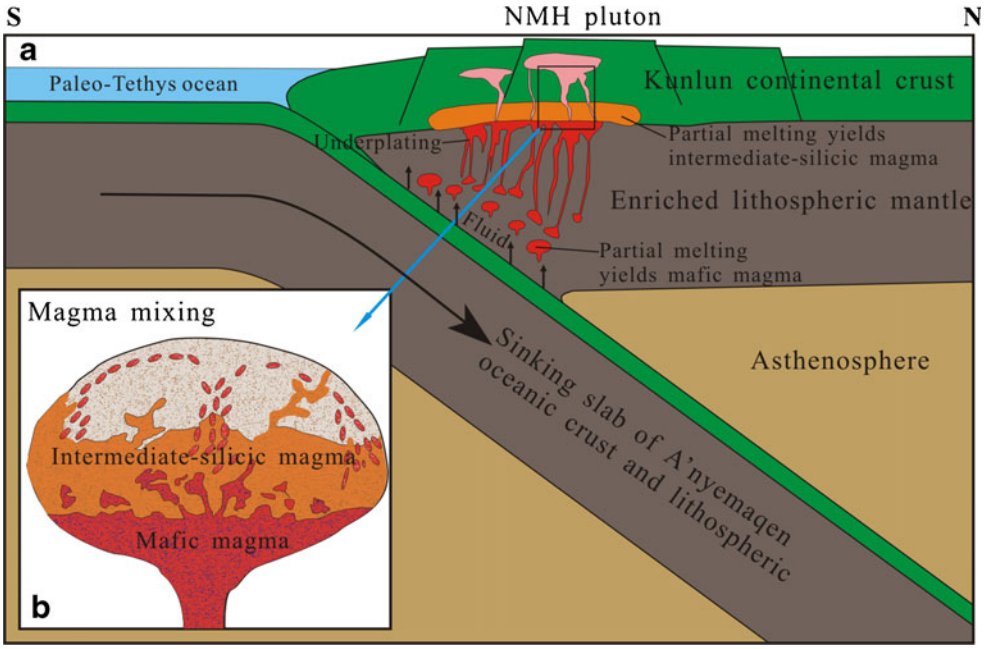


**Fig. 14** **a** Schematic illustration of magma generation in East Kunlun during slab subduction; **b** Schematic illustration of magma mixing during magma underplating

mafic magma sources, which is significantly different from Permian OIB rocks in Northern Qinghai-Tibet Plateau that derived from the asthenospheric mantle (Fig. 13).

Numerous studies of magma mixing in subduction zone environments have focused mainly on mafic rocks, such as basalts in the Andes (Debaille et al. 2006; Hickey et al. 1986; Hickey-Vargas et al. 2002), and concluded that the magma mixing involved melts from the subducted slab, the lithospheric mantle and the asthenospheric mantle. However, although this model may explain the petrogenesis of mafic rocks in subduction zones, it is not applicable to granodioritic or granitic rocks. Thus, MMEs are evidence for magma mixing involving melts from the lithospheric mantle and the overlying lower crust, which is an important mechanism of magma mixing in subduction zones and is applicable to the origin of large scale granitic magmatism, e.g., this study and Carboniferous enclave-rich granitoids of the Andes of central Chile (Parada et al. 1999).

With the A'nemaqen Paleo-tethys oceanic slab being subducted beneath the East Kunlun since ca. 260 Ma (Jiang et al. 1992; Yang et al. 1996), the fluid carried by the slab would induce partial melting of the mantle wedge, which is a major melting mechanism to form mafic magmas in subduction zones (McCulloch and Gamble 1991; Tatsumi and Kogiso 2003). We interpret this to be the reason why the studied rocks show enrichment in LILE and LREE, but are depleted in HFSE and HREE, since LILE and LREE remain are fluid mobile (McCulloch and Gamble 1991). Also, the presence of fluid could contribute to the progressive oxidation for the generation of amphibole crystals with a magnesio-hornblende core and an actinolite rim (Supplementary Table 3; Fig. 6; Martin 2007). Therefore, we suggest that the 260-Ma, subduction-related felsic magma (Naomuhun pluton) was derived from partial melting of Proterozoic crustal rocks, i.e., Xiaomiao group, which forms the basement of East Kunlun. This process was triggered by underplated melts derived from an enriched lithospheric mantle that formed MMEs (Fig. 14), just as the scenario in the Andes (Parada et al. 1999). Owing to the LILE- and LREE-rich fluid metasomatism, the mantle wedge underwent partial melting to form the underplated magma. This magma subsequently underplated the lower crust, and produced partial melts of felsic composition, which formed the NMH calc-alkaline granodiorites with mixed mantle component. A small volume of mafic magma derived from the enriched lithospheric mantle mixed with the granodioritic magma to form MMEs (Fig. 14b), which was then emplaced at a depth of ca. 12 km.

## Conclusions

(1) LA-ICPMS zircon U-Pb dating indicates that the NMH granodiorites crystallized at 261±2 Ma and the MMEs crystallized at 263±2 Ma. Thus, this magmatism took place close to the Lower-Upper Permian boundary during subduction of Paleo-Tethyan lithosphere.

(2) The MMEs and host granodiorites have identical mineral assemblages, similar mineral compositions, similar geochemical characteristics, indistinguishable Sr-Nd isotopic composition and almost simultaneous crystallization age, suggesting formation by magma mixing.

(3) The whole-rock geochemistry and Sr-Nd-Hf isotopic compositions indicate that mafic lower crust is the prime candidate for the source of the NMH granitoid rocks, and that the MMEs are products of magma mixing between lower crustal intermediate melts and mafic melts derived from the lithospheric mantle.

(4) The subduction-related calc-alkaline magmatism in the Northern Qinghai-Tibet Plateau, was caused by enriched lithospheric mantle-derived mafic magmas underplating the lower crust.

**Acknowledgments** This study was financially supported by China Geological Survey (Ke[2011]01-16-08 &1212010918002-13, Ke [2011]03-05-08&1212011121270), and National Nature Science Foundation of China (Grant 90814004). Thanks go to Chen Hai-hong, Zong Ke-qing and Chen Lu for their help with isotope laboratory chemistry. Also, we would like to thank Zheng Shu for his help during microprobe analyses. We are grateful to Professor Paul T. Robinson and Miguel Angel Parada for their constructive and helpful suggestions that led to considerable improvements in this manuscript. Besides, we acknowledge two journal reviewers for their constructive comments that helped improve the paper.

## References

Abdel-Rahman AFM (1994) Nature of biotites from alkaline, calc-alkaline, and peraluminous magmas. J Petrol 35:525–541

Anderson AT (1976) Magma mixing: petrological process and volcanological tool. J Volcanol Geoth Res 1:3–33

Arvin M, Dargahi S, Bababei AA (2004) Mafic microgranular enclave swarms in the Chenar granitoid stock, NW of Kerman, Iran: evidence for magma mingling. J Asian Earth Sci 24:105–113

Baier J, Audétat A, Keppler H (2008) The origin of the negative niobium tantalum anomaly in subduction zone magmas. Earth Planet Sci Lett 267:290–300

Batchelor RA, Bowden P (1985) Petrogenetic interpretation of granitoid rock series using multicationic parameters. Chem Geol 48:43–55

Baxter S, Feely M (2002) Magma mixing and mingling textures in granitoids: examples from the Galway Granite, Connemara, Ireland. Mineral Petrol 76:63–74

Bian QT, Li DH, Pospelov I, Yin LM, Li HS, Zhao DS, Chang CF, Luo XQ, Gao SL, Astrakhantsev O, Chamov N (2004) Age, geochemistry and tectonic setting of Buqingshan ophiolites, North Qinghai-Tibet Plateau, China. J Asian Earth Sci 23:577–596

Bievre DP, Taylor PD (1993) Table of the isotopic compositions of the elements. Int J Mass Spect Ion Proc 123:149–166

Blundy JD, Holland T (1990) Calcic amphibole equilibria and a new amphibole-plagioclase geothermometer. Contrib Mineral Petrol 104:208–224

Blundy JD, Sparks RSJ (1992) Petrogenesis of mafic inclusions in granitoids of the Adamello Massif, Italy. J Petrol 33:1039–1104

Brown GC, Thorpe RS, Webb PC (1984) The geochemical characteristics of granitoids in contrasting arcs and comments on magma sources. J Geol Soc Lond 141:413–426

Castro A, Moreno-Ventas I, de la Rosa JD (2006) Microgranular enclaves as indicators of hybridization processes in granitoid rocks, Hercynian Belt, Spain. Geol J 25:391–404

Chappel BW, White AJR (1974) Two contrasting granite types. Pacific Geol 8:173–174

Chen B, Wang Y (1996) Some characteristics of the orogenic belts in Qinghai-Tibet plateau. J SE Asian Earth Sci 13:237–242

Chen HW, Luo ZH, Mo XX, Liu CD, Ke S (2005) Underplating mechanism of Triassic granite of magma mixing origin in the East Kunlun orogenic belt. Geol Chin 32:386–395 (in Chinese with English abstract)

Chen NS, Wang XY, Zhang HF, Sun M, Li XY, Chen Q (2007) Geochemistry and Nd-Sr-Pb isotopic compositions of granitoids from Qaidam and Oulongbuluke micro-blocks, NW China: constraints on basement nature and tectonic affinity. J Chin Univ Geosci 32:7–21 (in Chinese with English abstract)

Chen XH, Yin A, Gehrels GE, Li L, Jiang RB (2011) Chemical geodynamics of granitic magmatism in the basement of the Eastern Qaidam basin, Northern Qinghai-Tibet Plateau. Acta Geol Sinica 85:157–171 (in Chinese with English abstract)

Chu NC, Taylor RN, Chavagnac V, Nesbitt RW, Boella RM, Milton JA, German CR, Bayon G, Burton K (2002) Hf isotope ratio analysis using multi-collector inductively coupled plasma mass spectrometry: an evaluation of isobaric interference corrections. J Anal At Spect 17:1567–1574

Coltorti M, Bonadiman C, Faccini B, Grégoire M, O'Reilly SY, Powell W (2007) Amphiboles from suprasubduction and intraplate lithospheric mantle. Lithos 99:68–84

Corfu F, Hanchar JM, Hoskin PWO, Kinny P (2003) Atlas of zircon textures. Rev Mineral Geochem 53:469–495

Debaille V, Doucelance R, Weis D, Schiano P (2006) Multi-stage mixing in subduction zones: Application to Merapi volcano (Java island, Sunda arc). Geochim Cosmochim Acta 70:723–741

Defant MJ, Drummond MS (1990) Derivation of some modern arc magmas by melting of young subducted lithosphere. Nature 347:662–665

Elhlou S, Belousova E, Griffin WL, Pearson NJ, O'Reilly SY (2006) Trace element and isotopic composition of GJ Red Zircon standard by laser ablation. Geochim Cosmochim Acta 70:A158

Forster MD (1960) Interpretation of the composition of trioctahedral micas. Geol Surv Prof Paper 354:11–49

Gao S, Rudnick RL, Yuan HL, Liu XM, Liu YS, Xu WL, Ling WL, Ayers J, Wang XC, Wang QH (2004) Recycling lower continental crust in the North China craton. Nature 432:892–897

Gardien V, Thompson AB, Grujic D, Ulmer P (1995) Experimental melting of biotite+plagioclase+quartz±muscovite assemblages and implications for crustal melting. J Geophys Res 100:15581–15591

Ginibre C, Wörner G, Kronz A (2007) Crystal zoning as an archive for magma evolution. Elements 3:261–266

Green TH (1995) Significance of Nb/Ta as an indicator of geochemical processes in the crust-mantle system. Chem Geol 120:347–359

Green TH, Pearson NJ (1987) An experimental study of Nb and Ta partitioning between Ti-rich minerals and silicate liquids at high pressure and temperature. Geochim Cosmochim Acta 51:55–62

Griffin WL, Pearson NJ, Belousova E, Jackson SE, van Achterbergh E, O'Reilly SY, Shee SR (2000) The Hf isotope composition of cratonic mantle: LAM-MC-ICPMS analysis of zircon megacrysts in kimberlites. Geochim Cosmochim Acta 64:133–147

Griffin WL, Wang X, Jackson SE, Pearson NJ, O'Reilly SY, Xu XS, Zhou XM (2002) Zircon chemistry and magma mixing, SE China: In-situ analysis of Hf isotopes, Tonglu and Pingtan igneous complexes. Lithos 61:237–269

Grogan SE, Reavy RJ (2002) Disequilibrium textures in the Leinster Granite Complex, SE Ireland: evidence for acid-acid magma mixing. Mineral Mag 66:929–939

Harris N, Xu RH, Lewis CL, Hawkesworth CJ, Zhang YQ (1988) Isotope geochemistry of the 1985 Tibet geotraverse, Lhasa to Golmud. Phil Trans R Soc Lond (A) 327:263–285

Hickey RL, Frey FA, Gerlach DC (1986) Multiple sources for basaltic arc rocks from the southern volcanic zone of the Andes (34°-41°S): trace element and isotopic evidence for contributions from subducted oceanic crust, mantle, and continental crust. J Geophys Res 91:5963–5984

Hickey-Vargas R, Sun M, López-Escobar L, Moreno-Roa H, Reagan MK, Morris JD, Ryan JG (2002) Multiple subduction components in the mantle wedge: evidence from eruptive centers in the Central Southern volcanic zone, Chile. Geology 30:199–202

Hoskin PWO, Schaltegger U (2003) The composition of zircon and igneous and metamorphic petrogenesis. Rev Mineral Geochem 53:27–55

Hu ZC, Gao S, Liu YS, Hu SH, Chen HH, Yuan HL (2008) Signal enhancement in laser ablation ICP-MS by addition of nitrogen in the central channel gas. J Anal At Spect 23:1093–1101

Hussain MF, Mondal MEA, Ahmad T (2004) Petrological and geochemical characteristics of Archean gneisses and granitoids from Bastar craton, Central India – implication for subduction related magmatism. Gondwana Res 7:531–537

Jackson SE, Pearson NJ, Griffin WL, Belousova EA (2004) The application of laser ablation-inductively coupled plasma-mass spectrometry to in situ U-Pb zircon geochronology. Chem Geol 211:47–69

Jiang CF, Yang JS, Feng BG, Zhu ZZ, Zhao M, Chai YC (1992) Opening-closing tectonic of Kunlun Mountains. Geological Publishing House, Beijing, pp 1–224, in Chinese

Kalfoun F, Ionov D, Merlet C (2002) HFSE residence and Nb/Ta ratios in metasomatised, rutile-bearing mantle peridotites. Earth Planet Sci Lett 199:49–65

Konstantinovskaia EA, Brunel M, Malavieille J (2003) Discovery of the Paleo-Tethys residual peridotites along the Anyemaqen–KunLun suture zone (North Tibet). CR Geosci 335:709–719

Leake BE, Wooley AR, Arps CES, Birch WD, Gilbert MC, Grice JD, Hawthorne FC, Kato A, Kisch HJ, Krivovichev VG (1997) Nomenclature of amphiboles: report of the Subcommittee on Amphiboles of the International Mineralogical Association, commission on new minerals and mineral names. Can Mineral 35:219–246

Lin WW, Peng LJ (1994) The estimation of $Fe^{3+}$ and $Fe^{2+}$ contents in amphibole and biotite from EMPA data. J Changchun Univ Earth Sci 24:155–162 (in Chinese with English abstract)

Liu CD, Zhang WQ, Mo XX, Luo ZH, Yu XH, Li SW, Zhao X (2002) Features and origin of mafic microgranular enclaves in the Yuegelu granite in the Eastern Kunlun. Geol Bull Chin 21:739–744 (in Chinese with English abstract)

Liu CD, Mo XX, Luo ZH, Yu XH, Chen HW, Li SW, Zhao X (2003) Pb-Sr-Nd-O isotope characteristics of granitoids in East Kunlun orogenic belt. Acta Geoscientica Sinica 24:584–588 (in Chinese with English abstract)

Liu CD, Mo XX, Luo ZH, Yu XH, Chen HW, Li SW, Zhao X (2004) Mixing events between the crust-and mantle-derived magmas in Eastern Kunlun: evidence from zircon SHRIMP chronology. Chin Sci Bull 49:828–834

Liu YS, Hu ZC, Gao S, Günther D, Xu J, Gao CG, Chen HH (2008) In situ analysis of major and trace elements of anhydrous

minerals by LA-ICP-MS without applying an internal standard. Chem Geol 257:34–43
Ludwig KR (2003) Isoplot 3.00: A geochronological toolkit for Microsoft Excel. Berkeley Geochronology Center, California
Ma CQ, Wang RJ, Qiu JX (1992) Enclaves as indicators of the origin of granitoid magma and repeatet magma mingling: an example from the Zhoukoudian intrusion, Beijiing. Geol Rev 38:109–119 (in Chinese with English abstract)
Ma LY, Niu ZJ, Bai YS, Duan QF, Wang JX (2007) Sr, Nd and Pb isotopic geochemistry of Permian volcanic rocks from southern Qinghai and their geological significance. J Chin Univ Geosci 32:22–28 (in Chinese with English abstract)
Maniar PD, Piccoli PM (1989) Tectonic discrimination of granitoids. Geol Soc Am Bull 101:635–643
Martin RF (2007) Amphiboles in the igneous environment. Rev Mineral Geochem 67:323–358
McCulloch MT, Gamble JA (1991) Geochemical and geodynamical constraints on subduction zone magmatism. Earth Planet Sci Lett 102:358–374
Middlemost EAK (1994) Naming materials in the magma/igneous rock system. Earth Sci Rev 37:215–224
Mock C, Arnaud NO, Cantagrel JM (1999) An early unroofing in northeastern Tibet? Constraints from $^{40}Ar/^{39}Ar$ thermochronology on granitoids from the eastern Kunlun range (Qianghai, NW China). Earth Planet Sci Lett 171:107–122
Omrani J, Agard P, Whitechurch H, Benoit M, Prouteau G, Jolivet L (2008) Arc-magmatism and subduction history beneath the Zagros Mountains, Iran: a new report of adakites and geodynamic consequences. Lithos 106:380–39
Pal T, Mitra SK, Sengupta S, Katari A, Bandopradhyay PC, Bhattacharya AK (2007) Dacite-andesites of Narcondam volcano in the Andaman Sea: an imprint of magma mixing in the inner arc of the Andaman-Java subduction system. J Volcanol Geoth Res 168:93–113
Parada MA, Nyström JO, Levi B (1999) Multiple sources for the Coastal Batholith of central Chile (31–34°S): geochemical and Sr-Nd isotopic evidence and tectonic implications. Lithos 46:505–521
Patiño Douce AE (1997) Generation of metaluminous A-type granites by low-pressure melting of calc-alkaline granitoids. Geology 25:743–746
Pearce JA, Harris NBW, Tindle AG (1984) Trace element discrimination diagrams for the tectonic interpretation of granitic rocks. J Petrol 25:956–983
Peccerillo A, Taylor SR (1976) Geochemistry of Eocene calc-alkaline volcanic rocks from the Kastamonu area, northern Turkey. Contrib Mineral Petrol 58:63–81
Pietranik A, Koepke J (2009) Interactions between dioritic and granodioritic magmas in mingling zones: plagioclase record of mixing, mingling and subsolidus interactions in the Gęsiniec Intrusion, NE Bohemian Massif, SW Poland. Contrib Mineral Petrol 158:17–36
Qin JF, Lai SC, Diwu CR, Ju YJ, Li YF (2010) Magma mixing origin for the post-collisional adakitic monzogranite of the Triassic Yangba pluton, Northwestern margin of the South China block: geochemistry, Sr–Nd isotopic, zircon U–Pb dating and Hf isotopic evidences. Contrib Mineral Petrol 159:389–409
Rapp RP, Watson EB (1995) Dehydration melting of metabasalt at 8–32 kbar: implications for continental growth and crust-mantle recycling. J Petrol 36:891–931
Roger F, Jolivet M, Malavieille J (2008) Tectonic evolution of the Triassic fold belts of Tibet. CR Geosci 340:180–189
Schmidt MW (1992) Amphibole composition in tonalite as a function of pressure: an experimental calibration of the Al-in-hornblende barometer. Contrib Mineral Petrol 110:304–310
Slaby E, Götze J (2004) Feldspar crystallization under magma-mixing conditions shown by cathodoluminescence and geochemical modelling - a case study from the Karkonosze pluton (SW Poland). Mineral Mag 68:561–577
Stern CR, Kilian R (1996) Role of the subducted slab, mantle wedge and continental crust in the generation of adakites from the Andean Austral Volcanic Zone. Contrib Mineral Petrol 123:263–281
Streck MJ, Leeman WP, Chesley J (2007) High-magnesian andesite from Mount Shasta: a product of magma mixing and contamination, not a primitive mantle melt. Geology 35:351–354
Sun SS, McDonough WF (1989) Chemical and isotopic systematics of oceanic basalts: implications for mantle composition and processes. Geol Soc London Spec Publ 42:313–345
Tatsumi Y, Kogiso T (2003) The subduction factory: its role in the evolution of the Earth's crust and mantle. Geol Soc London Spec Publ 219:55–80
Taylor SR, McLennan SM (1985) The continental crust: Its composition and evolution. Blackwell Scientific Publications, Oxford
Tobisch OT, McNulty BA, Vernon RH (1997) Microgranitoid enclave swarms in granitic plutons, central Sierra Nevada, California. Lithos 40:321–339
Wade BP, Barovich KM, Hand M, Scrimgeour IR, Close DF (2006) Evidence for early mesoproterozoic arc magmatism in the musgrave block, Central Australia: implications for proterozoic crustal growth and tectonic reconstructions of Australia. J Geol 114:43–63
Wang GC, Jia CX, Zhu YH, Lin QX, Xiang SY (2003) Regional geological survey report of People's Republic of China (on a scale of 1:250 000, Alake lake sites). China University of Geosciences Press, Wuhan (in Chinese)
Wiedenbeck M, Alle P, Corfu F, Griffin WL, Meier M, Oberli F, Quadt AV, Roddick JC, Spiegel W (1995) Three natural zircon standards for U-Th-Pb, Lu-Hf, trace element and REE analyses. Geostand Geoanal Res 19:1–23
Woodhead JD, Hergt JM (2005) A preliminary appraisal of seven natural zircon reference materials for in situ Hf isotope determination. Geostand Geoanal Res 29:183–195
Wu YB, Zheng YF (2004) Genesis of zircon and its constraints on interpretation of U-Pb age. Chin Sci Bull 49:1554–1569
Xu ZQ, Yang JS, Li HB, Zhang JX, Wu CL (2007) Orogenic plateaux: Terrane amalgamation, collision and uplift in the Qinghai-Tibet plateau. Geological Publishing House, Beijing, pp 176–181, in Chinese
Yang JS, Robinson PT, Jiang CF, Xu ZQ (1996) Ophiolites of the Kunlun Mountains, China and their tectonic implications. Tectonophysics 258:215–231
Yang JS, Xu ZQ, Li HB, Shi RD (2005) The paleo-Tethyan volcanism and plate tectonic regime in the A'nyemaqen region of East Kunlun, northern Tibet Plateau. Acta Petrol Mineral 24:369–380 (in Chinese with English abstract)
Yang JH, Wu FY, Chung SL, Wilde SA, Chu MF (2006) A hybrid origin for the Qianshan A-type granite, northeast China: geochemical and Sr-Nd-Hf isotopic evidence. Lithos 89:89–106
Yang JH, Wu FY, Wilde SA, Liu XM (2007a) Petrogenesis of late triassic granitoids and their enclaves with implications for post-collisional lithospheric thinning of the Liaodong Peninsula, North China Craton. Chem Geol 242:155–175
Yang JH, Wu FY, Wilde SA, Xie LW, Yang YH, Liu XM (2007b) Tracing magma mixing in granite genesis: in situ U–Pb dating and Hf-isotope analysis of zircons. Contrib Mineral Petrol 153:177–190
Yang JS, Shi RD, Wu CL, Wang XB, Robinson PT (2009) Dur'ngoi ophiolite in East Kunlun, Northeast Tibetan plateau: evidence for paleo-Tethyan suture in Northwest China. J Earth Sci 20:303–331
Yu N, Jin W, Ge WC, Long XP (2005) Geochemical study on peraluminous granite from Jinshuikou in East Kunlun. Global Geol 24:123–128 (in Chinese with English abstract)
Yuan HL, Gao S, Dai MN, Zong CL, Günther D, Fontaine GH, Liu XM, Diwu CR (2008) Simultaneous determinations of U-Pb age,

Hf isotopes and trace element compositions of zircon by excimer laser-ablation quadrupole and multiple-collector ICP-MS. Chem Geol 247:100–118

Yuan C, Sun M, Xiao WJ, Wilde S, Li XH, Liu XH, Long XP, Xia XP, Ye K, Li JL (2009) Garnet-bearing tonalitic porphyry from East Kunlun, Northeast Tibetan Plateau: implications for adakite and magmas from the MASH Zone. Int J Earth Sci 98:1489–1510

Zheng S, Hu ZC, Shi YF (2009) Accurate determination of Ni, Ca and Mn in olivine by EPMA and LA-ICP-MS. J Chin Univ Geosci 34:220–224 (in Chinese with English abstract)

Zong KQ, Liu YS, Gao CG, Hu ZC, Gao S, Gong HJ (2010) In situ U–Pb dating and trace element analysis of zircons in thin sections of eclogite: refining constraints on the ultra-high pressure metamorphism of the Sulu terrane, China. Chem Geol 269:237–251